Zhang *et al. EURASIP Journal on Wireless Communications and Networking* (2018) 2018:246
https://doi.org/10.1186/s13638-018-1261-8

EURASIP Journal on Wireless Communications and Networking

RESEARCH Open Access

Channel autocorrelation-based dynamic slot scheduling for body area networks

Hongyun Zhang[1,2*], Farzad Safaei[1] and Le Chung Tran[1]

Abstract

As a promising technology in the context of m-health and e-medical, wireless body area networks (WBANs) have a stringent requirement in terms of transmission reliability. Meanwhile, the wireless channel in WBANs is prone to deep fading due to multiple reasons, such as shadowing by the body, reflection, diffraction, and interference. To meet the challenge in transmission reliability, the dynamic slot scheduling (DSS) methods have attracted considerable interest in recent years. DSS method does not require extra hardware or software overhead on the sensor side. Instead, the hub optimizes the time-division multiple access slots by selecting the best permutation at the beginning of each superframe to improve the transmission reliability. However, most existing DSS works optimize the time slot scheduling based on a two-state ("good" or "bad") Markov channel model, which is insufficient for human daily life scenarios with a variety of irregular activities. In this paper, we first collect the channel gain data in the real human daily scenarios and analyze the autocorrelation of wireless channels based on this real database. Motivated by the significant temporal autocorrelation, we then propose a new DSS method, which applies a temporal autocorrelation model to predict the channel condition for future time slots. The new method is designed to be compatible with IEEE 802.15.6 standard. Compared to the classical Markov model-based methods, simulation results show that the newly proposed DSS method achieves up to 12.9% reduction in terms of packet loss ratios.

Keywords: Dynamic slot scheduling, Channel autocorrelation, Scheduled access, Wireless body area networks, IEEE 802.15.6

1 Introduction

Wireless body area networks (WBANs) are radio networks of sensors and/or actuators, placed on, in, or around the human body, and represent the latest generation of personal area networks [1]. The development of WBANs is of great importance for a wide range of applications, including healthcare, emergency services, sports, and consumer entertainment. However, due to the peculiarities of WBAN channels, WBANs still face many challenges in the medium access control (MAC) layers.

One of the crucial challenges is ensuring the transmission reliability for major WBAN-based applications, such as e-health and patient care. Different from other typical wireless radio channels, a large number of factors may result in the severe attenuation (over 100 dB has been observed) in WBAN channels. These factors include diffraction, reflection, energy absorption and consumption, antenna losses, shadowing by the body tissue, and body posture [2–7]. It has been demonstrated by many research works, such as [8, 9], that the shadowing effect from the human body is the dominant factor that leads to the severe attenuation. Moreover, the deep fading effect in WBANs might last from 10 to 300 ms [10, 11], which is longer than cellular networks. On the other hand, constrained by the miniaturization of WBAN sensor nodes, both energy supply and processing/storage capacity are very limited. Therefore, designing a reliable and efficient data transmission strategy for WBANs becomes imperative to promote the prevalence of WBANs.

In recent years, many dynamic schemes which adjust key transmission parameters in accordance with the real-time channel state or application requirements have been proposed to meet the transmission challenges in WBANs. Among these works, adaptive duty cycle (ADC) [12–15] and transmission power control (TPC) [16–22] are the

*Correspondence: hz697@uowmail.edu.au
[1]School of Electrical, Computer and Telecommunications Engineering, University of Wollongong, Northfields Ave, 2522 Wollongong, Australia
[2]Artificial Intelligence Research Center, National Innovation Institute of Defense Technology, 10091 Beijing, China

two key research topics. However, both ADC and TPC methods require additional hardware or software cost on the sensor side. In this paper, we will focus on the dynamic slot scheduling (DSS) method, which dynamically optimizes the permutation of time slots in each superframe. Because of the advantages in collision-free and energy efficiency, the TDMA-based approach is put forth as one of the most appropriate MAC solutions. However, due to the high volatility of on-body channels, a simple static TDMA allocation may lead to significant waste. Specifically, if a time slot is assigned to a particular sensor node with a bad channel to the hub (coordinator or sink), the data packets from this sensor are prone to be lost. However, the slot cannot be used by any other node that may have a good link. This not only wastes the energy but also decreases the throughput. Ideally, we would like to allocate a transmission slot to a sensor node only when the state of its link to the hub allows a successful data transfer. The core idea of DSS method is scheduling the time slots according to the variation of link conditions rather than a fixed scheduling. It is worth noting that all the additional controls are added to the hub, and there is no increase in sensors' complexity.

The core idea of DSS has been somewhat mentioned in the literature, which is usually referred to as "opportunistic scheduling" in the context of cellular networks [23]. However, traditional opportunistic scheduling approaches are not compatible with WBAN systems as they require that the slave nodes are continuously available for communication [9]. This requirement is unacceptable for the energy-constrained sensors, which are in a sleep mode most of the time. Besides, most opportunistic scheduling methods for cellular networks do not consider the peculiarities of WBAN channels, e.g., high variation and predominant shadowing from the body.

Recently, some DSS works are proposed in the context of WBANs. In [24, 25], the authors use a two-state ("good" or "bad") Gilbert model [26] to describe the variation of on-body channels. Based on the Markov channel model, a DSS scheme, named *flipping*, is proposed to maximize the expected number of successful transmissions in a TDMA round. The flipping scheme schedules all bad links of the previous superframe last and preserves the order in time in which they were observed while schedules all good links first but reversing the order in which they were observed in the previous superframe. The rationale behind flipping method is that all bad links are given the longest time to recover (i.e., getting out of the outage), while the flipped ordering of the good links takes advantage of the most recently observed good links to ensure a high probability of success in the next transmissions round. Some other research works are also based on the assumption of two-state Markov channel model. To tackle the dynamic fluctuation of on-body channels, the work in [27] presents a novel transition matrix estimation method. In [28], the authors focus on adapting the slot order to improve the effectiveness of retransmission. The node with the worst channel condition is scheduled to occupy the first time slot to get the highest chance of discovering a relaying node, and the best channel is scheduled at the last. In [29–31], the authors propose a flipping-like scheduling approach which also adopts Gilbert model to describe the on-body channel. Besides, the Quality of Service (QoS) requirements, including energy efficiency, data rate, and packet reception rate, are taken into account to optimize not only the slot order but also slot number.

However, the main limitation of these Markov model-based schemes is that the condition of on-body links is limited to only two states: good and bad, which are insufficient to describe the on-body channel states in the complex WBAN application scenarios, especially the daily scenarios with mixed activities. Besides, these studies do not consider the correlation between links. In fact, due to the variability of human movements and postures, the independent Markov process is insufficient to model the on-body channels.

In this study, motivated by the significant temporal autocorrelation of the on-body channels in the human daily activity scenarios, a temporal autocorrelation-based DSS method (DSS-TA) is proposed. DSS-TA utilizes a temporal autocorrelation model to estimate the on-body channel condition for future time slots and then optimizes the permutation of scheduled time slots for all connected sensor nodes based on the estimation results. The new method is designed to be compatible with the IEEE 802.15.6 standard [1].

The major contributions of this paper are as follows:

- We collect the channel realizations in the real daily life scenarios with mixed activities. Then, we offer insight into the autocorrelation of on-body channels and point out that there is an untapped potential for leveraging the significant autocorrelation features for DSS in WBANs.
- We first propose to utilize a temporal autocorrelation model to optimize the slot scheduling and detail its implementation in the IEEE 802.15.6. The new method jointly takes the latest and historical channel states into consideration, thus achieving a more accurate prediction of channel conditions.
- We evaluate the performance of our DSS-TA method through importing the real channel realizations into the simulation model. Simulation results show that, compared to conventional DSS methods, the newly proposed DSS method achieves up to 12.9% reduction in terms of packet loss ratios.

The rest of the paper is organized as follows. Section 2 provides the autocorrelation analyses of on-body channels with the experimental investigation. Then, the system model and problem formulation are presented in Section 3. Section 4 details the newly proposed DSS-TA method. Performance evaluation results based on the real channel realizations are presented in Section 5. Finally, Section 6 concludes the paper.

2 On-body channel measurement and autocorrelation analysis

2.1 Measurement setups

In this paper, a one-hop star topology composed of one hub and five sensors is considered. The deployment of the transceivers is depicted in Fig. 1, where the transmitter (acting as the hub) is placed on the abdomen and five receivers (acting as sensor nodes) are mounted on limbs and head. The receiver mounted on the left wrist is named as SN_{LW}. Corresponding to the positions of the other receivers, the other four receivers are named as SN_{RW} (right wrist), SN_{LA} (left ankle), SN_{RA} (right ankle), and SN_{H} (head).

The wireless transceivers work at the 2.4 GHz ISM band, which is one of the candidate carrier frequencies for the IEEE 802.15.6 BAN standard [1]. The wireless transceivers are assembled by commercial components, which are easy to build. The structure of the portable transceiver is shown in Fig. 2. The main function of these transceivers is to transmit and receive continuous data packets to/from each other and record the received signal strength indicator (RSSI) values into a micro SD card. More detailed description of the hardware can be found in [6–8].

When the measurement begins, the transmitter continuously broadcasts sample packets to the five receivers with the transmission (Tx) power of 0 dBm, and the sample packet transmission frequency is 200 Hz (i.e., sending 200 packets per second). Upon receiving the sample packet, the receivers record the packet sequence number, the timestamp, and the RSSI value into a text trace file. If the gap of sequence numbers between two successive sample packets, which a receiver receives successfully, exceeds one, some packets between these two packets have been lost due to the severe channel condition. In this case, the records of these lost packets will be added to the trace file with RSSI = − 100 dBm. It should be mentioned that the RSSI values can be less than − 100 dBm. The value − 100 dBm is chosen as a reference value to indicate a severe channel condition that would result in the packet loss. Taking the case in Fig. 3 as an example, the hub broadcasts four sample packets ($Pkt_{16} - Pkt_{19}$) to the sensors nodes, but SN_{LW} only receives two packets (Pkt_{16} and Pkt_{19}) and loses two packets (Pkt_{17} and Pkt_{18}). Accordingly, after receiving Pkt_{19}, SN_{LW} will add two more data rows in the trace file with RSSI = − 100 dBm, i.e., the middle two records in the data file of Fig. 3. In addition, as the Tx power is set to 0 dBm, the RSSI value can be considered as the channel gain and the inverse of the RSSI is the path loss.

In this study, we focus on mixed activities encountered in typical daily scenarios, so the measurement environments include indoor office, gym, home, walkway, and car. Meanwhile, we do not limit the types of activities that the test subjects should conduct. These activities include standing, walking, jogging, running, sitting, driving, and many other irregular movements. Two male subjects and two female subjects are invited to conduct the measurements. Each test subject conducts four measurements on four different days. For each measurement, the test subject is required to wear six wireless transceivers for 1 h, and the subject continues their daily life just like every other normal day. Corresponding to the five receivers, each measurement produces five trace files, each of which stores 72×10^4 records (200 packets/second × 3600 s). Each trace file is a channel realization for one particular channel, e.g., from the hub to SN_{LW}. The five trace files collected from one measurement form one dataset, and we refer to each dataset as a channel dataset. Since 16 measurements are conducted, there are 16 channel datasets in total, and they are named CD_1 to CD_{16}, respectively.

2.2 Channel autocorrelation

Next, these channel realizations collected from the daily scenarios are used to characterize the temporal autocorrelation of the on-body channels. Specifically, the autocorrelation coefficients of each channel for time delay from 5 to 500 ms are calculated. The following equation is adopted to evaluate the autocorrelation

$$\gamma(k) = \frac{\sum_{n=1}^{N-k}\left(G(n)-\bar{G}\right)\left(G(n+k)-\bar{G}\right)}{\sum_{n=1}^{N}(G(n)-\bar{G})^2} \tag{1}$$

where $\bar{G}$ is the mean value of N channel gain (or RSSI) values, i.e., $\{G(1), G(2)\ldots G(N)\}$, and k is the time shifting index in the record sequence. As the sampling frequency in our experiment is 200 Hz, k also represents a time lag of $k\times5$ ms. As demonstrated in [32], the on-body channel may not satisfy the wide-sense stationary (WSS) assumption when the time window is longer than 500 ms. Hence, in this paper, we focus on exploring the autocorrelation within a time lag of 500 ms, i.e., k is set from 1 to 100. N is the size of channel gain (or RSSI) data points, which is 72×10^4 for each on-body channel when the whole channel realization records are considered.

First, two channel datasets are picked to show the autocorrelation variation between different links and different test subjects. Figure 4 shows the autocorrelation coefficients of the five on-body channels. The results displayed in Fig. 4a are calculated based on the first channel dataset

Fig. 1 The deployment of transceivers

performed by the male subject 1, i.e., CD_1, and the results of Fig. 4b correspond to the first channel dataset from the female subject 1, i.e., CD_9. In Fig. 4, γ_{rw} represents the autocorrelation coefficient of channel "SN_{RW}-Hub." Correspondingly, γ_h, γ_{lw}, γ_{la}, and γ_{ra} represent the autocorrelation coefficient for channel "SN_H-Hub," "SN_{LW}-Hub," "SN_{LA}-Hub," and "SN_{RA}-Hub," respectively. Clearly, due to the variations of activities, environment, and sensor position, the autocorrelation of on-body channels varies with the change of test subject and the

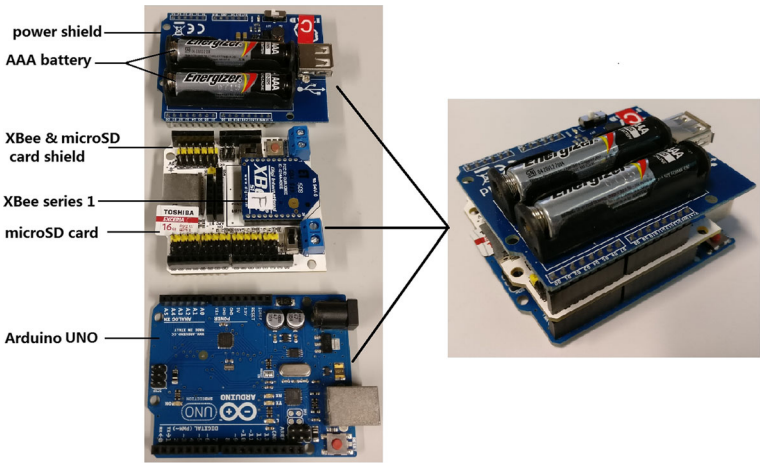

Fig. 2 Components of the portable transceiver

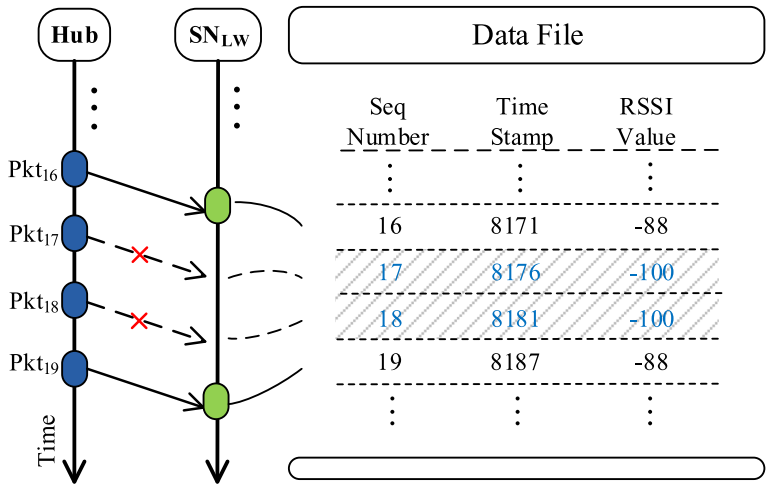

Fig. 3 Channel data recording when packets are lost

location of the receiver. On the one hand, there are clear distinctions between the autocorrelation curves for different channels. On the other hand, the autocorrelation coefficient for a certain channel also varies in different channel realizations. For example, the autocorrelation coefficient of channel "SN_{RW}-Hub" (denoted as γ_{rw}) drops rapidly with the increase of time lag in CD_1. Whereas, γ_{rw} exhibits a much smoother and smaller decline in CD_9.

However, in spite of the discrepancy resulting from different test subjects and different sensor positions, all five on-body channels exhibit significant autocorrelation characteristics within a time lag of 500 ms. To have more insights into the on-body channel autocorrelation, we explore the ensemble average of autocorrelation coefficient over all 16 channel datasets. As shown in Fig. 5, $\bar{\gamma}_h$, $\bar{\gamma}_{lw}$, $\bar{\gamma}_{rw}$, $\bar{\gamma}_{la}$, and $\bar{\gamma}_{ra}$ represent the ensemble average of autocorrelation coefficient for channel "SN_H-Hub," "SN_{LW}-Hub," "SN_{RW}-Hub," "SN_{LA}-Hub," and "SN_{RA}-Hub," respectively. If the coherence time is defined as the period when the autocorrelation coefficient is above 0.7, the average coherence times for the five on-body channels all exceed 500 ms, which is much longer than the coherence time in the monotone walking or running activity scenarios [33] (23–73 ms). The main reason may be because the daily scenarios are mixed with multiple activities, but most activities are relatively static, e.g., standing and sitting. More specifically, the channel between the torso and the head exhibits the most striking autocorrelation. It is mainly because the relative distance as well as the shadowing effect in this channel are more stable than the other four channels. Besides, the channels between the torso and two ankles show a more significant autocorrelation than the channels between the torso and two wrists. The main reason for this phenomenon may be because the movement of the upper limbs is more drastic than the lower limbs.

In summary, the autocorrelation of on-body channels varies with the change of test subject and the location of receiver. However, in the daily scenarios, the on-body channels exhibit a significant autocorrelation within a time lag of 500 ms. This general characteristic may provide a great potential in channel condition estimation. This untapped feature has inspired us to optimize the TDMA slot schedule as mentioned in this paper. In addition, due to the dynamic variation of body's shadowing effect and reflection from surrounding objects, the autocorrelation for a specific on-body channel on a certain subject fluctuates in the timeline. Accordingly, if we want to predict the channel condition by using the on-body channel autocorrelation, the autocorrelation coefficient should be kept up to date. The detail of channel information collection mechanism and real-time autocorrelation calculation will be presented in Section 4.

3 System model and problem formulation

3.1 System model

In this paper, we consider a one-hop star topology composed of one hub and a number of sensors. As the health monitoring is considered as the application of interest, all sensors periodically upload data packets to the hub. In the MAC layer, the MAC model of the IEEE 802.15.6 standard [1] is adopted. In the IEEE 802.15.6 standard, a hub shall operate in three types of access modes: beacon mode with superframes, non-beacon mode with superframes, and non-beacon mode without superframes. As the beacon mode with superframes provides the most flexible option in terms of access phases, we consider this mode in this paper. As shown in Fig. 6, one active superframe

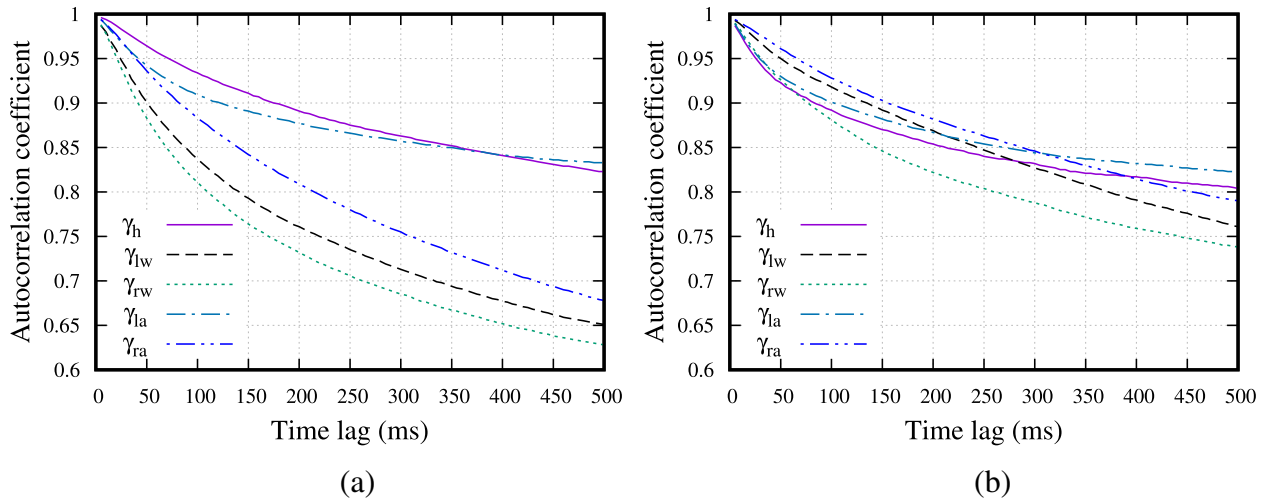

Fig. 4 The autocorrelation in two typical channel datasets. **a** Channel dataset (CD_1). **b** Channel dataset 9 (CD_9)

(beacon period) consists of two access phases: random access phase (RAP1) and managed access phase (MAP). Both RAP1 and MAP consist of several time slots with the same length, i.e., T_s. In the RAP1, the carrier sense multiple access/collision avoidance (CSMA/CA) access method is performed to exchange management and control packets, including the connection request and assignment packets. In the MAP, the TDMA access method is utilized to schedule the upload interval for sensor nodes. After the scheduling of the hub, the exclusive upload intervals for the sensor nodes are located in the MAP. For brevity, we call the exclusive interval as SUI, i.e., scheduled upload interval. In this study, we assume that the hub assigns the same length of SUI to each sensor in one superframe, and we call this constraint as "fairness constraint." It is worth noting that for comparison, we also consider the method which the hub allocates the time slots only based on the channel condition, without the restriction of the equal SUI length. However, as will be presented in Section 5, there exists a significant imbalance in the data rate of different sensors in the latter case. For the radio layer, all wireless devices operate in a half-duplex mode and no relay nodes are used in the network. All sensors are configured with the same Tx power level. As the hub device is usually less energy-constrained, the Tx power level of the hub is higher than that of sensors. Therefore, the downlink channels (from the hub to the sensors) are assumed to be much more reliable than the uplink channels (from the sensors to the hub).

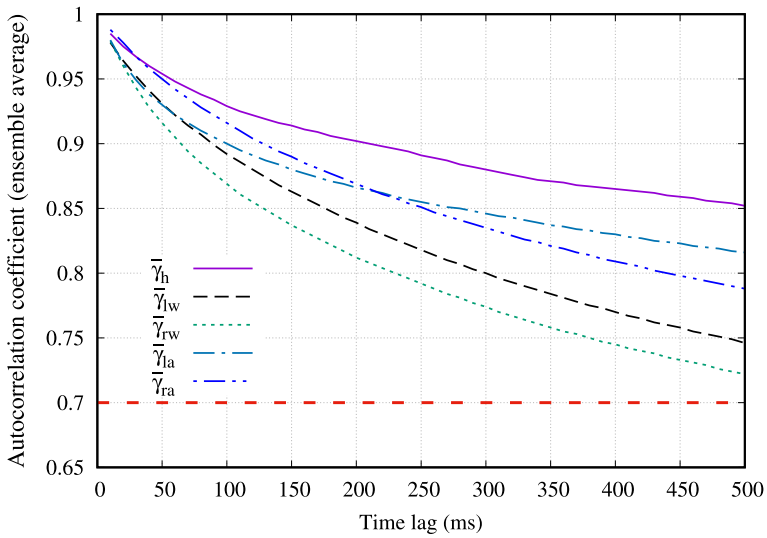

Fig. 5 Ensemble average autocorrelation vs. time lag

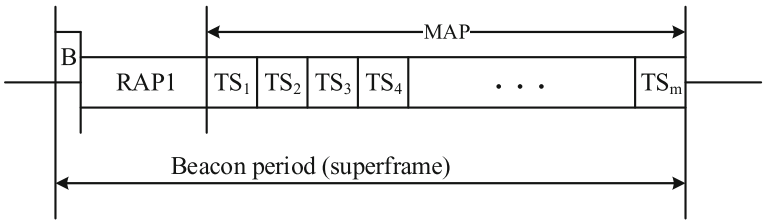

Fig. 6 Superframe structure

3.2 Problem formulation

In the classical TDMA method, upon accomplishing the scheduling in the first TDMA round, the order of SUI for all sensor nodes will remain the same in the following TDMA rounds. However, some time slots may be occupied by a sensor with a bad channel condition to the hub. These time slots cannot be assigned to another sensor that may have a better link. Moreover, as the sensor is assigned to an interval with a bad channel condition, it also loses the opportunity to have a good channel condition in another interval. Unlike the static TDMA method, DSS methods focus on the problem of how to dynamically schedule the time slots in each superframe. Ideally, DSS methods aim to allocate transmission slots to a sensor only when the state of its link to the hub allows a successful data transfer.

Assuming there are n sensors ($\mathrm{SN}_1 - \mathrm{SN}_n$) in the network, and each MAP is split into m slots with the same duration (cf. Fig. 6), denoted as $\mathrm{TS}_1, \mathrm{TS}_2, \ldots, \mathrm{TS}_m$. Each sensor node is assigned with q slots to upload data packets in MAP, so there are $\lfloor m/q \rfloor$ available intervals. We denote $K(i)$ as the SUI assigned to SN_i, $1 \leqslant K(i) \leqslant \lfloor m/q \rfloor$, and vector $\mathbf{K} = (K(1), K(2), ..., K(n))$ represents the SUI permutation in one MAP. Theoretically, the total number of possible values of $\mathbf{K}$ is the n-permutation of $\lfloor m/q \rfloor$, i.e., $\prod_{i=0}^{n-1}(\lfloor m/q \rfloor - i)$, for each superframe. In DSS methods, the $\mathbf{K}$ does not remain the same across different superframes, which is the key different compared to a static TDMA assignment. Let us consider the example in Fig. 7. Assuming there are three sensors in the network and five time slots in one MAP, each sensor is assigned one time slot, i.e., $m = 5$, $n = 3$, and $q = 1$. In the previous beacon period, TS_2, TS_1, and TS_4 are assigned to SN_1, SN_2, and SN_3, respectively, i.e., $\mathbf{K} = (2, 1, 4)$. In static TDMA method, $\mathbf{K}$ remains the same for all TDMA rounds. The problem of DSS methods lies on how to choose the optimal value of vector $\mathbf{K}$ for current superframe based on the historical channel information.

The main target of all DSS methods is to minimize the packet loss from the sensors to the hub. More specifically, at the start of each superframe, the permutation of SUI for the current superframe should be optimized based on the following criteria:

$$\min_{\vec{K}} \sum_{i=1}^{n} p_i(K(i)) \quad \text{for } i \neq j,\ K(i) \leqslant \lfloor m/q \rfloor \text{ and } K(i) \neq K(j) \tag{2}$$

where $p_i(K(i))$ represents the average packet loss ratio (PLR) of the link "SN_i-Hub" in the $K(i)$th time interval. Since the number of intervals is $\lfloor m/q \rfloor$ and $K(i)$ denotes the SUI assigned to SN_i, we have the first constraint, i.e., $K(i) \leqslant \lfloor m/q \rfloor$. Besides, the second constraint $K(i) \neq K(j)$ is provided as two sensors possess two independent SUIs. Based on Eq. (2), the more accurate estimation of $p_i(K(i))$, the better performance of the DSS method. However, estimating the full channel state information at the start of each round is not trivial, especially in the dynamic WBAN scenarios. The key challenge of DSS schemes is how to predict the channel conditions by using the channel information from the previous superframes and then optimizing the time slot scheduling in the current superframe based on the prediction results.

4 The proposed DSS-TA method

In the proposed DSS-TA method, the hub predicts the channel condition based on a temporal autocorrelation model at the beginning of each superframe. Specifically, DSS-TA consists of three parts: channel information collection, PLR prediction, and slot permutation optimization. Except for the first part that needs the assistance of sensor nodes, DSS-TA is mainly implemented on the hub side, which is considered to be less constrained by energy, storage, and computation resources.

4.1 Channel information collection

As presented in Eq. (1), historical channel gains are needed at the granularity of time slots to calculate the latest autocorrelation coefficient. Intuitively, the hub could collect the channel conditions by receiving the upload packets from the sensor nodes. However, every sensor node only uploads the data packets during their SUI, which misses the channel information during the other time slots. Meanwhile, if multiple sensor nodes simultaneously upload packets to the hub, it may result in severe

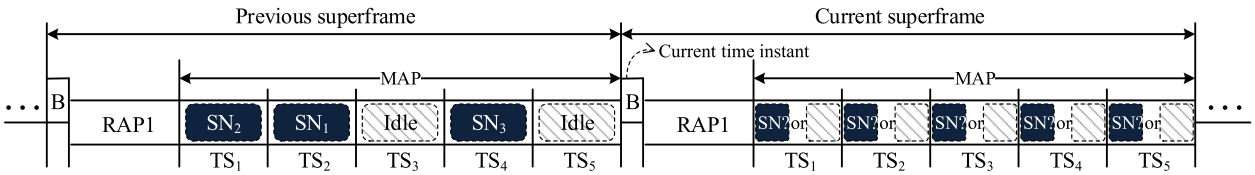

Fig. 7 Time slot scheduling problem

signal collisions. Therefore, broadcast from the hub to all sensors, i.e., downlink transmission, is used to track the channel condition. As demonstrated in [34, 35], the on-body channels show prominent reciprocity in narrowband communication environments, which means the channel profiles of downlink and uplink are about the same. Therefore, the channel gain of uplink channels can be estimated by the measurement of the downlink channel. Specifically, the hub keeps broadcasting control or sample packets to all sensors, then the sensor nodes will feedback the RSSI values to the hub during their SUIs.

Consider an example in Fig. 8. There are five time slots ($TS_1 - TS_5$) in the MAP, and three sensor nodes ($SN_1 - SN_3$) are assigned one time slot each. In order to record the channel gain for each time slot, we introduce an extra subslot in the tail of each time slot. On the hub side, depending on whether the current time slot is free or not, the hub shall broadcast one control or sample data packet, respectively, to all sensor nodes in the extra subslot. If the current time slot is assigned to a sensor (i.e., $TS_1 - TS_3$ in Fig. 8), the hub shall broadcast a B-Ack packet during the extra subslot. The B-Ack packet means block acknowledgment packet, which is combined with the block acknowledgment later (L-Ack) packet to support the L-Ack &B-Ack acknowledgment policy of IEEE 802.15.6. In DSS-TA, L-Ack & B-Ack policy is adopted in the uplink data transmission. That means the Ack policy field of all data packets would be set to L-Ack, except the last data packet in each time slot which is set to B-Ack. On the other hand, if the current time slot is set as free (TS_4 and TS_5 in Fig. 8), instead of broadcasting the acknowledgment packet, the hub shall broadcast a sample packet to all sensor nodes during the extra subslot. At the sensor side, if the current time slot is assigned to a certain sensor, this sensor will stay in a normal active state. Otherwise, the sensor will be in the sleep state. During the extra subslots, three sensor nodes will stay in Rx (reception) state to receive B-Ack or sample packets from the hub. Upon

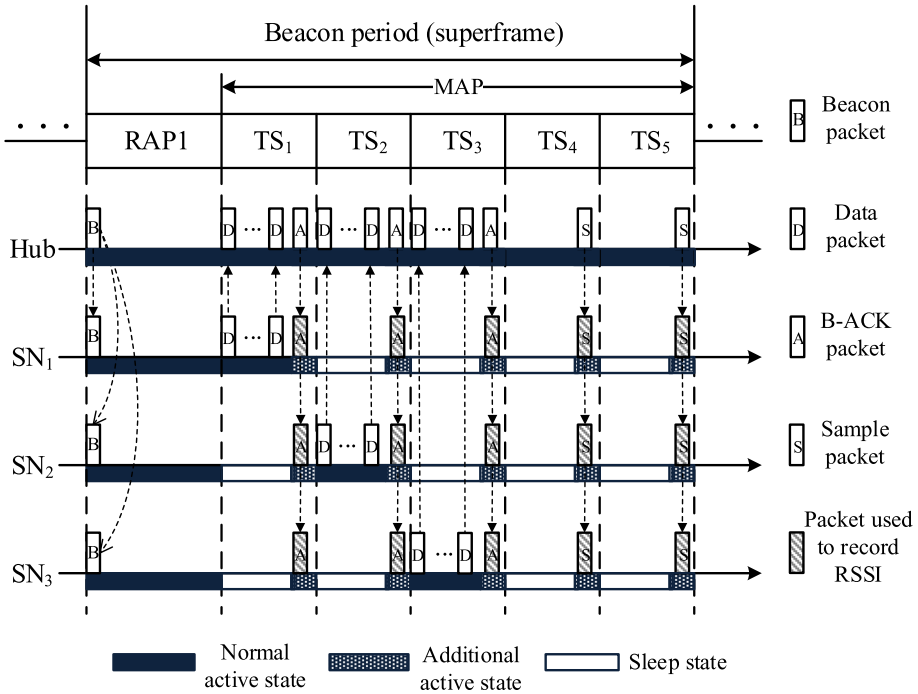

Fig. 8 Channel information collection

receiving the B-Ack or sample packet from the hub, the sensor nodes record the RSSI values and assemble them into the headers of data packets, which would be uploaded during the next superframe. Note that the hub knows the Tx power level of the B-Ack or sample packets; thus, it is easy to calculate the channel gain (or path loss) after receiving the historical RSSI values. By this approach, the hub keeps track of the channel conditions of each channel in every time slot, while the sensor nodes only stay active during the extra subslots and its allocated interval.

In DSS-TA, the hub stores the channel gain data of the latest 2 s, which contain 400 channel gain values for each sensor. Note that, choosing an appropriate sample size to estimate the autocorrelation is not a trivial task. On the one hand, with the increase of sample size, more data points are utilized to calculate the channel autocorrelations, which may appear to result in a more accurate estimation of autocorrelation. On the other hand, since the sampling frequency is fixed, a bigger sample size means these data points are collected from a wider time span. However, as demonstrated in [32], on-body channels show a low probability of WSS assumption outside the time span of 500 ms. In other words, the timeliness of autocorrelation calculation is weakened with the increase of sample size. In fact, there exists a trade-off between accuracy and timeliness when choosing the sample size. We will explore the effect of the sample size in Section 5.

4.2 Packet loss ratio prediction

We first introduce the temporal autocorrelation model used to predict the PLR. Suppose the sensor node SN_i transmits a data packet to the hub with the transmission power P_{Tx}, and the hub receives the packet with the power P_{Rx}. Then, the channel gain for the channel "SN_i-Hub" is defined as

$$G_i|_{dB} = P_{Rx}|_{\text{dBm}} - P_{Tx}|_{\text{dBm}}. \tag{3}$$

Meanwhile, as proved in [34, 36–38], the lognormal distribution provides a good fit for the long-term average on-body channel gain. Therefore, the channel gain in the channel "SN_i-Hub" can be described by a Gaussian random variable (r.v.)

$$G_i|_{dB} \sim \mathcal{N}\left(\mu_i, \sigma_i^2\right), \tag{4}$$

where μ_i and σ_i are the mean and standard deviation of the channel gain, respectively. Note that both μ_i and σ_i depend directly on the type of human activity, the position of transmitting and receiving nodes, and propagation environment. In this study, we assume the variation of the channel gain is a WSS process within 500 ms; thus, μ_i and σ_i remain the same within 500 ms. Accordingly, the channel gains within this period follow the same distribution

$$G_i\left(T_0\right) \sim \mathcal{N}\left(\mu_i, \sigma_i^2\right), \tag{5}$$

$$G_i\left(T_0+\tau\right) \sim \mathcal{N}\left(\mu_i, \sigma_i^2\right) \quad \tau \leqslant 500\ \text{ms} \tag{6}$$

where $G_i(T_0)$ and $G_i(T_0+\tau)$ are the channel gains at the time instants T_0 and $T_0+\tau$, respectively. Therefore, the joint distribution of the two channel gains recorded at different time instants can be expressed as [39]

$$\left(G_i\left(T_0\right), G_i\left(T_0+\tau\right)\right) \sim \mathcal{N}\left(\mu_i, \mu_i, \sigma_i^2, \sigma_i^2, \rho_i(\tau)\right) \tag{7}$$

where $\rho_i(\tau)$ denotes the autocorrelation coefficient for a time lag of τ. Furthermore, the conditional distribution of $G_i(T_0+\tau)$ can be deduced to [39]:

$$G_i\left(T_0+\tau\right) \sim \mathcal{N}\left(\left(1-\rho_i(\tau)\right)\mu_i + \rho_i(\tau)G_i\left(T_0\right), \left(1-\rho_i^2(\tau)\right)\sigma_i^2\right). \tag{8}$$

The PLR is the probability of the received signal power below the pre-defined receiving power threshold. Thus, the PLR for the time instant $T_0+\tau$ is given by

$$\begin{aligned} p_i\left(T_0+\tau\right) &= \text{Prob}\left(P_{Rx}\left(T_0+\tau\right) \leqslant {P_{Rx}}^*\right) \\ &= \text{Prob}\left(G_i\left(T_0+\tau\right) + P_{Tx}\left(T_0+\tau\right) \leqslant {P_{Rx}}^*\right) \\ &= \text{Prob}\left(G_i\left(T_0+\tau\right) \leqslant G^*\right) \end{aligned} \tag{9}$$

where $p_i(T_0+\tau)$ is the PLR, $P_{Tx}(T_0+\tau)$ and $P_{Rx}(T_0+\tau)$ are the signal transmitting and receiving power, respectively, ${P_{Rx}}^*$ is the pre-defined receiving power threshold, and $G^* = {P_{Rx}}^* - P_{Tx}(T_0+\tau)$ is defined as the channel gain threshold. Consequently, combining Eqs. (8) and (9), $p_i(T_0+\tau)$ can be predicted by

$$\begin{aligned} p_i\left(T_0+\tau\right) &= \int_{-\infty}^{G^*} f_{G_i(T_0+\tau)}\left(G_i\right) dG_i \\ &= \Phi\left(\frac{G^* - \left(1-\rho_i(\tau)\right)\mu_i - \rho_i(\tau)G_i\left(T_0\right)}{\sigma_i\sqrt{\left(1-\rho_i^2(\tau)\right)}}\right) \end{aligned} \tag{10}$$

where $f_{G_i(T_0+\tau)}(G_i)$ is the probability density function of $G_i(T_0+\tau)$ and $\Phi(\cdot)$ is the cumulative distribution function of the standard normal distribution.

Equations (8)–(10) are called as the temporal autocorrelation model (TAM), which is first proposed in [39]. In [39], the TAM model is used to choose dynamically between the relay and direct transmissions. In DSS-TA, the collected historical channel gain data is combined with TAM at the hub side to predict the PLR for each channel.

Based on Eq. (10), the following parameters: $G_i(T_0)$, μ_i, σ_i, and $\rho_i(\tau)$ are required in the hub side. Firstly, the latest channel gain record in the previous superframe is chosen as $G_i(T_0)$. Then, the channel gain expectation μ_i and standard deviation σ_i can be estimated by the sample mean ($\hat{\mu}_i$) and sample standard deviation ($\hat{\sigma}_i$)

$$\hat{\mu}_i = \bar{G}_i = \frac{1}{n}\sum_{x=1}^{n} G_i(x) \tag{11}$$

$$\hat{\sigma}_i = \sqrt{\frac{1}{n}\sum_{x=1}^{n}\left(G_i(x) - \bar{G}_i\right)^2} \tag{12}$$

where $G_i(x)$ $(x = 1, 2, \ldots, n)$ are the historical channel gain records, and $n = 400$ is the sample size. Next, we will calculate the autocorrelation coefficient $\rho_i(\tau)$. We convert the time lag of τ to the number of time slots, i.e., $\lfloor \tau / T_s \rfloor$. Hence, $\rho_i(\tau)$ can be estimated as $\gamma_i(\lfloor \tau / T_s \rfloor)$, based on Eq. (1). In addition, in order to predict the channel condition for multiple future time slots, the hub should calculate an autocorrelation coefficient vector for each channel. In DSS-TA, the autocorrelation coefficients within the time lag of 500 ms are calculated. For instance, if the length of one time slot is 5 ms, each autocorrelation vector has $500/5 = 100$ elements, which are denoted for the channel "SN_i-Hub" as $\vec{\gamma_i} = (\gamma_i(1), \gamma_i(2), \gamma_i(3), \ldots, \gamma_i(100))$. Besides, when the time lag exceeds 500 ms, the autocorrelation coefficient is considered as $\gamma_i(100)$.

4.3 Slot permutation optimization

As presented in Eq. (2), the aim of DSS approaches is to find a permutation of SUI, i.e., **K**, to minimize the sum of PLR of all links. In fact, the process of finding an optimal **K** for the current superframe can be converted into a minimum-cost matching problem in a bipartite graph. The bipartite graph can be denoted as $G = (U, V, E)$, where U and V denote the sensor node set and time interval set, respectively, E denotes the edges between the two subsets. In the DSS-TA, the cost of the edge from the sensor SN_i to the time interval x, namely TI_x, is weighted by the average PLR of the link "SN_i-Hub" during TI_x. If each sensor is assigned with q time slots, the length of one time interval equals $q \times T_s$, and the predicted PLR for one time interval is estimated as the mean value of q predicted PLR values within that time interval. Accordingly, using the PLR prediction algorithm mentioned before, a $|U| \times |V|$ adjacency matrix can be built to represent the bipartite graph, and the entries of the matrix are all estimated PLR values. $|U|$ and $|V|$ denote the size of the sets U and V, respectively. The assignment problem in the bipartite graph can be solved by the Hungarian algorithm [40], which is also called as Kuhn-Munkres algorithm. In addition, the time complexity in the worst cases of this algorithm is $O(J^3)$, $J = \max\{n, \lfloor m/q \rfloor\}$, where n is the number of sensors and $\lfloor m/q \rfloor$ is the number of time intervals. Considering both n and m are below 256 [1], this complexity is acceptable.

Figure 9 illustrates the process of finding the minimum-cost matching. There are three sensor nodes in the network and five time slots in one MAP, and suppose each sensor is assigned with one time slot, i.e., $n = |U| = 3$, $m = |V| = 5$, and $q = 1$. Figure 9a presents the predicted PLR matrix for the current superframe. The entry at the coordinate (a, b) denotes the predicted average PLR for the channel "SN_a-Hub" during TS_b. By performing the Hungarian algorithm on this matrix, the selected edges are depicted in Fig. 9b. The optimal slot scheduling is that TS_5, TS_4, and TS_1 are assigned to SN_1, SN_2, SN_3 respectively, i.e., $\mathbf{K} = (5, 4, 1)$. The cases when $q > 1$ are similar, except that the cost of each edge is the mean value of q predicted PLR values within the considered time interval.

In short, at the start of each beacon period, the hub performs the PLR prediction algorithm to predict the PLRs for each time interval in the MAP and then performs the Hungarian algorithm to calculate the optimal permutation vector **K**. Then, the optimal **K** is inserted into the beacon packet, which would be broadcasted to all sensor nodes. Upon receiving the beacon packet, sensor nodes obtain their exclusive upload intervals, set radio state timer, and control their data uploading process in the scheduled time slots.

5 Performance evaluation

In this section, we evaluate the performance of the proposed DSS-TA. To do that, we build a simulation model as follows. The channel datasets collected from our measurement campaigns are imported into the simulation model to represent the variation of actual on-body channels in the daily scenarios. To demonstrate the effectiveness of DSS-TA, we compare the performance of the DSS-TA method with the following methods.

1. **Static TDMA:** The uplink time slots of all sensors are fixed after being assigned in the first superframe. The order of sensors' SUIs is chosen randomly in the first superframe.
- **Random:** Unlike the static approach, the random scheme re-schedules the time slots at the start of each superframe, and the permutation of SUI is selected randomly.
2. **Flipping:** The flipping method schedules all "bad" links of the previous superframe last, preserving the order in time in which they were observed. Meanwhile, it schedules all "good" links first but reversing the order in which they were observed in the previous superframe. The original flipping [24, 25] method assumes the number of sensors is identical to the number of available upload intervals. In this section, we consider a more general version where the number of available upload intervals may be larger than the number of sensors. Accordingly, some slots located in the middle of the MAP may remain idle.
3. **Perfect prediction:** This scheme is designed to explore the upper bound of DSS approaches. The hub is assumed to know exactly the channel gain of any time slot in the next beacon period. Therefore, the perfect prediction method can optimize the assignment based on the accurate value of channel gain. This method is infeasible for real WBAN

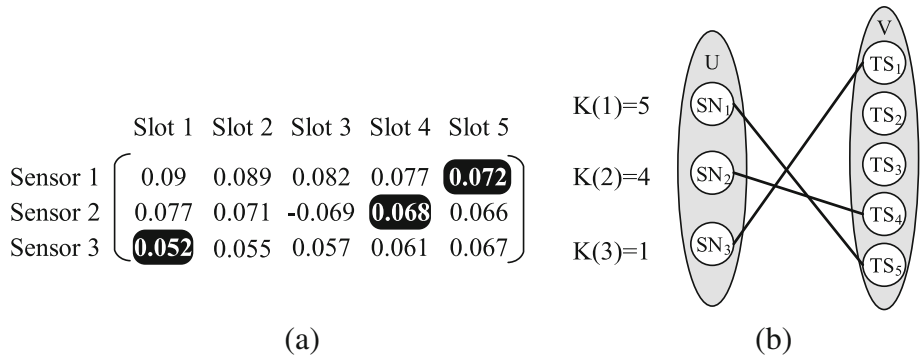

Fig. 9 An example of finding the minimum cost matching. **a** predicted PLR matrix. **b** selected minimum edges

systems because it assumes perfect prediction of future states.

4. **Fairness unconstrained:** Unlike all the aforementioned methods, this method does not restrict the SUI length for the sensors. A sensor may obtain the whole time slots if the channel condition from the sensor to the hub is predicted as the best during the MAP. On the other hand, another sensor may not be allocated any time slot to upload packets due to its bad channel conditions. For the purpose of comparison, the fairness unconstrained method adopts the PLR prediction mechanism which we propose in the DSS-TA method. The hub adopts a greedy strategy to schedule the time slots, each time slot is assigned to the sensor with the lowest predicted PLR.

5.1 Simulation model and configurations

We build the simulation model from wireless channels to the application layer based on the Castalia framework [41]. Compared to other simulators, Castalia provides more realistic network features, such as accurate realistic radio model, clock drift, and energy consumption model. All the important default parameters of the protocol stack and hardware are listed in Table 1. In the wireless channel layer, the "TraceChannel" model is selected, in which the on-body channels are simulated by the channel datasets collected from our measurement campaign, i.e., CD_1, CD_2, …, CD_{16}. Corresponding to the 16 channel datasets, we carry 16 simulations for each simulation configuration by importing different channel datasets to the simulation model. Because each channel realization lasts 3600 s (1 h), the simulation time is also set to 3600 s. The functions of application and routing layer are relatively simple. The application layer generates sample data packets with the rate of "PacketRate," and the routing layer forwards packets between the application layer and MAC layer. In the MAC layer, one time slot is set to 5 ms. The 4-ms period

Table 1 Simulation parameters for DSS-TA

Parameter	Value
Application layer	
PacketSize	87 bytes
PacketRate	30 Pkts/s
Routing layer	
PacketOverhead	10 bytes
MAC layer	
SuperframeLength	70 ms
RAP1Length	10 ms
SlotLength	5 ms
SubslotLength	1 ms
SUI	10 ms
pTIFS	0.03 ms
Data's AckType	L-Ack & B-Ack
Control's AckType	I-Ack
PacketOverheader	7 bytes
Radio layer	
dataRate	250 kbps
modulationType	PSK
bandwidth	20 MHz
carrierFreq	2400.0 MHz
noiseFloor	– 101 dBm
sensitivity	– 95 dBm
CCAthreshold	– 95 dBm
symbolsForRSSI	8 bits
Tx Power	– 15 dBm
FrameOverheader	6 bytes
pTimeSleepToTx	0.05 ms
pTimeSleepToRx	0.05 ms
Others	
Wireless channel	TraceChannel
simulationTime	3600 s

in the front is used for uploading data packets, and the 1-ms period at the end is the extra subplot used for receiving B-Ack or sample packets from the hub. As for the radio layer, all the parameters are set based on a low power RF transceiver module CC2420 [42]. Besides, taking the overheads of different layers into account, the size of one data frame is 110 bytes (87 + 10 + 7 + 6); hence, the transmission delay for one frame is $(110 \times 8)/250 = 3.52$ ms (the transmission rate is 250 Kbits/s). Taking the guard time and pSIFS (short interframe separation time) into account, the sensor nodes only transmit one data packet in one time slot.

5.2 Simulation results

As mentioned before, there exists a trade-off between accuracy and timeliness when choosing the sample size in DSS-TA. By presenting the relationship between the PLR and the sample size, we explore the best sample size for daily scenarios. Four channel datasets collected from four test subjects, i.e., CD_1, CD_5, CD_9, and CD_{13}, are selected as the examples to show the PLR as a function of the sample size. As shown in Fig. 10, the PLR reaches the minimum when the sample size is about 400. Since the sampling frequency of our measurements is 200 Hz, 400 data points corresponding to the time duration of 2 s. The accuracy of autocorrelation estimation is weakened by a sample size smaller than 400. On the other hand, when the sample size is bigger than 400, the PLR increases slightly. The reason is that, when the time duration is longer than 2 s (corresponding to 400 data points), the non-stationary property of on-body channels starts to offset the accuracy despite having more data points, leading to an increase of the PLR. Accordingly, the latest 400 channel gain values are chosen as the sample data points to perform the PLR prediction algorithm in both the proposed DSS-TA and the fairness unconstrained method.

Next, the comparison between the DSS-TA method and the fairness unconstrained method is presented. The comparison will explain the reason for introducing the "fairness constraint," where all sensors shall have the same length of SUI in each MAP. Taking four typical channel datasets (CD_1, CD_5, CD_9, and CD_{13}) as the examples, the upload data rate for each sensor and average data rate are depicted in Fig. 11. As expected, the fairness unconstrained method exhibits a better performance in terms of the average data rate. However, in most cases, the fairness unconstrained method shows a significant discrepancy of data rates between different sensor nodes. We consider the significant discrepancy as "unfairness" between sensors. Specifically, SN_{RW}, SN_{RA}, and SN_{LA} are severely starved in CD_1, CD_9, and CD_{13}, respectively. In other words, the discrepancy of data rates between different sensor nodes could be significant and unpredictable in the fairness unconstrained method. If the WBAN application aims at the maximum average data rate and does not require a minimum data rate for the sensor nodes, the fairness unconstrained method may be the best choice. However, the unpredictable and significant discrepancy is not suitable for the majority WBAN applications. This is the rationale for introducing the "fairness constraint" in this paper.

The following simulations will focus on the comparison among four DSS methods, namely the static, random,

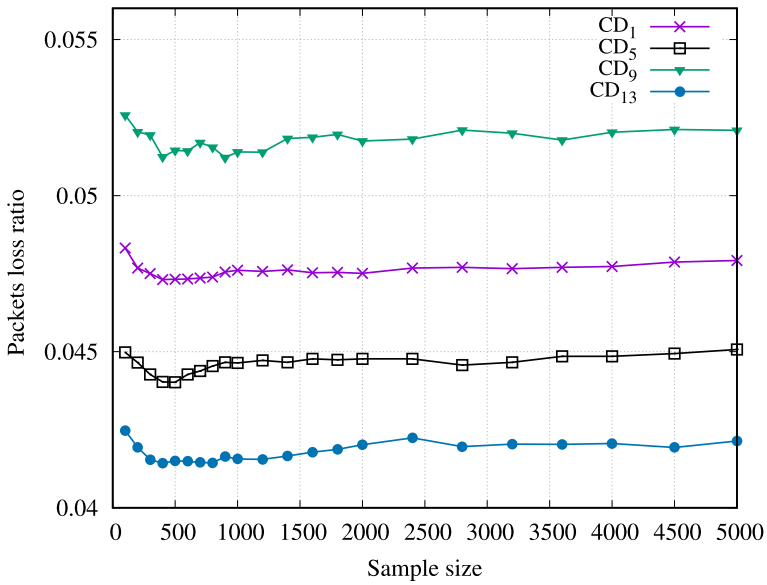

Fig. 10 Packet loss ratio vs. sample size in DSS-TA: superframe = 70 ms, Tx power = – 15 dBm

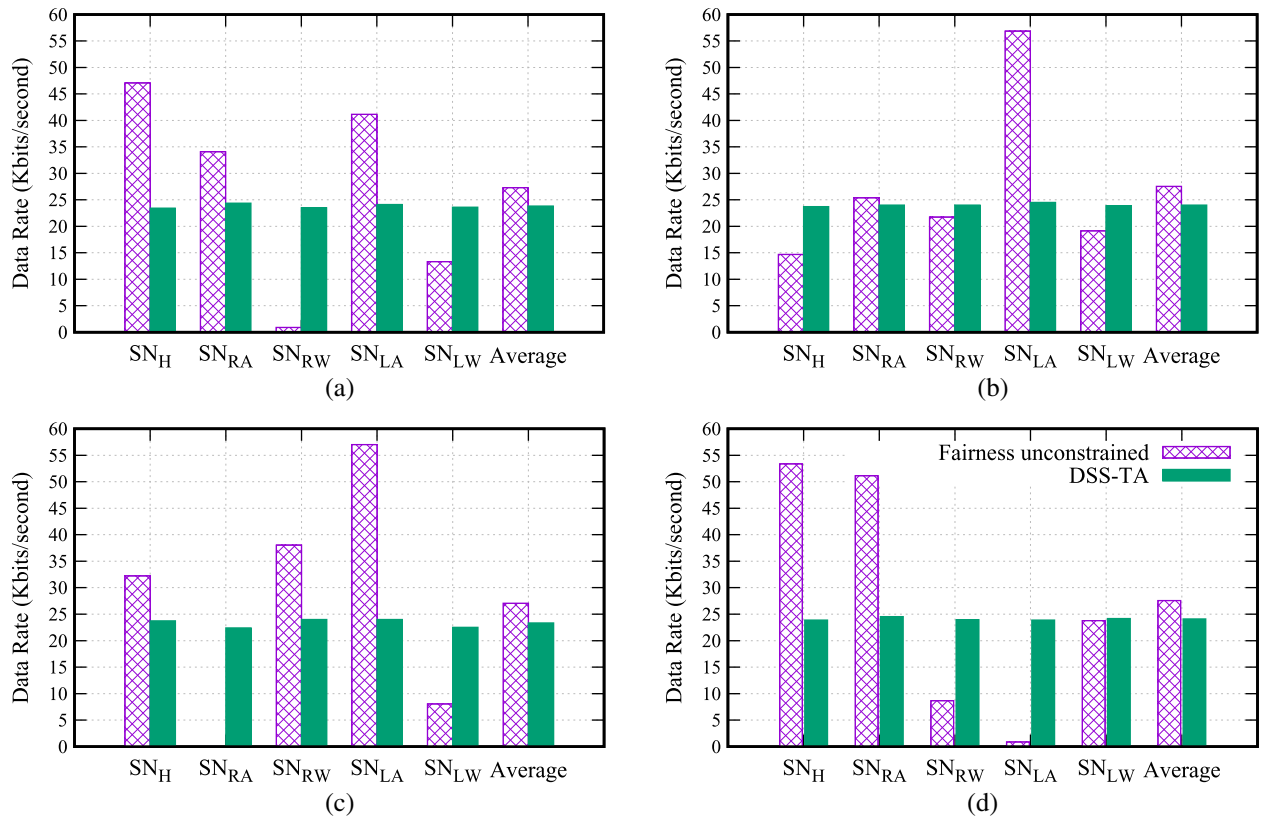

Fig. 11 The comparison of upload data rate between DSS-TA and the fairness unconstrained method, superframe length 70 ms, $P_{Tx} = -15$ dBm. **a** Channel dataset 1 (CD_1). **b** Channel dataset 5 (CD_5). **c** Channel dataset 9 (CD_9). **d** Channel dataset 13 (CD_13)

flipping, perfect prediction, and newly proposed DSS-TA methods under the "fairness constraint." Since these schemes comply with the "fairness constraint," the data rates of all sensors would be roughly the same. Hence, the average upload packet loss ratio is considered to be the main performance metric. We first explore the PLR performance when adopting different levels of Tx power. Clearly, boosting the Tx power can decrease the PLR, but also increases the power consumption, which is strictly limited in WBAN systems. On the other hand, a low Tx power may cause the PLR to exceed the guideline of PLR in WBAN system. As summarized in [43], a PLR less than 10% is considered as a guideline in this study. Accordingly, we set the range of Tx power from -18 to -8 dBm. Figure 12 shows the PLR performance of different scheduling methods by importing the first channel dataset CD_1 into the simulation model. As expected, the PLR decreases with the increase of Tx power. The proposed DSS-TA is significantly better than the static, flipping, and random methods. Specifically, compared to the flipping method, DSS-TA achieves a 9.6–12.7% reduction in terms of PLR.

Figure 13 shows the mean and standard deviation of PLR reduction over the static method for the four DSS methods, namely the random, flipping, perfect prediction, and DSS-TA. Note that the PLR reduction over the static method represents the percentage of the improvement in terms of PLR, compared to the static method, defined as $(\mathrm{PLR}_{\mathrm{static}} - \mathrm{PLR}_{\mathrm{DSS}})/\mathrm{PLR}_{\mathrm{static}}$. Clearly, DSS-TA achieves a much better PLR reduction (6.43–10.28%) in comparison with the conventional flipping method (0–2.89%). Figure 13 also shows that the PLR reduction of DSS-TA is more significant when the Tx power is higher.

The superframe length (the duration of one beacon period) is another key parameter. We now focus on exploring the PLR as a function of the superframe length. To avoid a significant decrease in throughput when extending the superframe length, we prolong the SUI for sensors with the extension of the superframe length. Specifically, we allocated one more time slot (5 ms) to each sensor when the superframe length is augmented by 35 ms. Figure 14 presents the simulation results by importing the first channel dataset CD_1, while Fig. 15 illustrates the mean and standard deviation of the PLR reduction over the static method.

From Figs. 14 and 15, we have the following observations. Firstly, as expected, the PLR performances of both

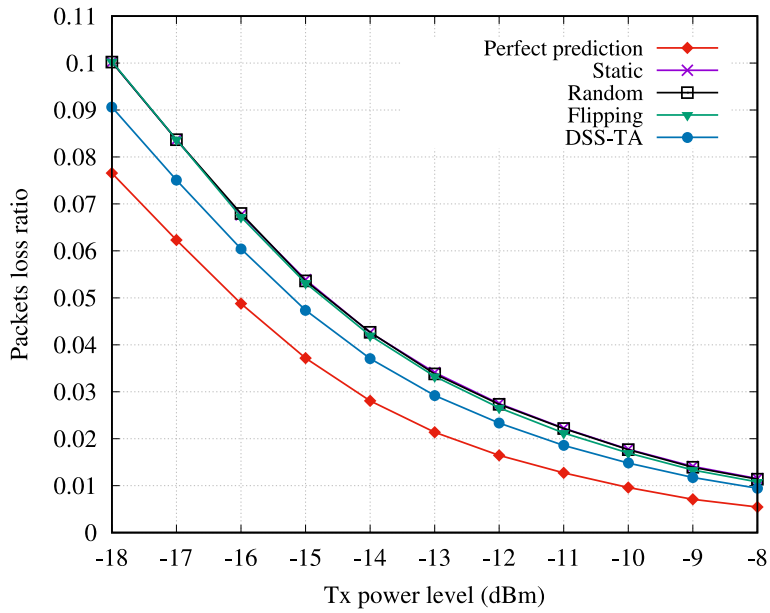

Fig. 12 PLR vs. Tx power lever: superframe length 70 ms, CD_1

static and random methods do not change with the extension of the superframe length. Secondly, the performance of the perfect prediction method continuously improves with the extension of the superframe length. The reason may be the "bad" channel has a longer time to recover when a longer superframe length is adopted. Besides, since the perfect prediction scheme represents the upper bound performance of DSS methods, this observation also indicates that DSS methods have more potential when a longer superframe is adopted. Thirdly, the performance of DSS-TA slightly improves when the superframe length increases from 35 to 105 ms. Specifically, for the channel dataset CD_1, DSS-TA achieves the best PLR performance when the superframe length is 105 ms, which is about

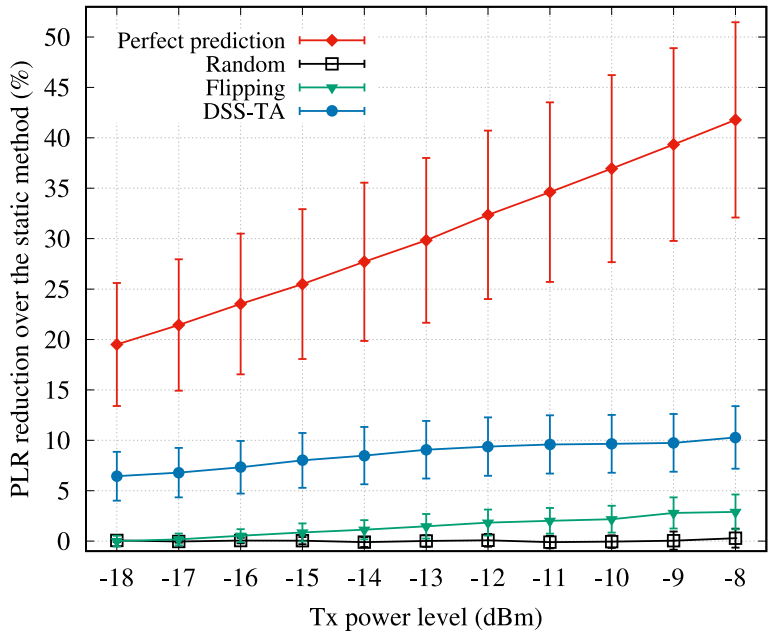

Fig. 13 PLR reduction over the static method vs. Tx power level, superframe length 70 ms

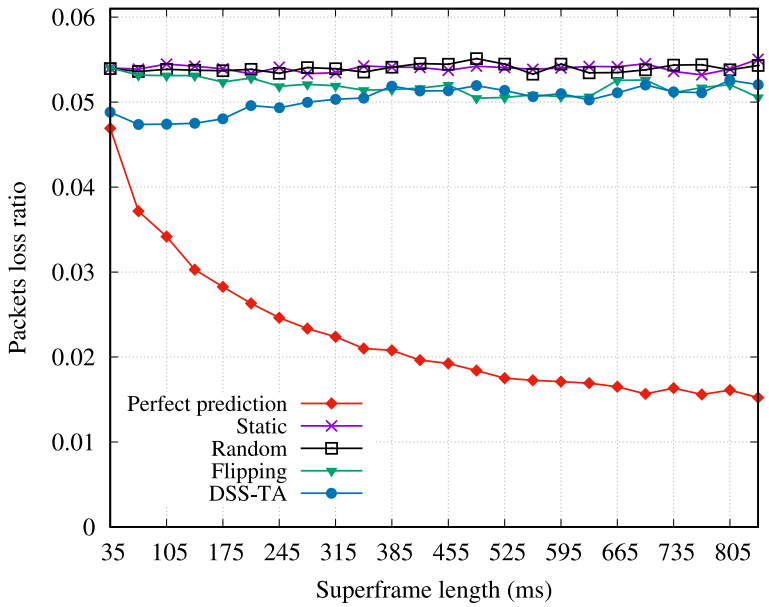

Fig. 14 PLR vs. superframe length, $P_{Tx} = -15$ dBm, CD_1

10.9% PLR reduction in comparison with the flipping method. Then, the further prolongation of superframe would undermine the effectiveness of DSS-TA. On the one hand, when the superframe is too short, there is not enough time to "revive" the bad channels, even the TAM model could provide an accurate PLR prediction. On the other hand, the channel autocorrelation decreases with the extension of the superframe length. Thus, the accuracy of PLR prediction results also decreases when a longer superframe is adopted, which decreases the performance of DSS-TA. At last, we found that when the superframe length is larger than 490 ms, the flipping and DSS-TA methods achieve the roughly same performance. Compared to the flipping method, the TAM used in the DSS-TA considers not only the latest channel gains but also the channel gains in the past 2 s. Therefore, this

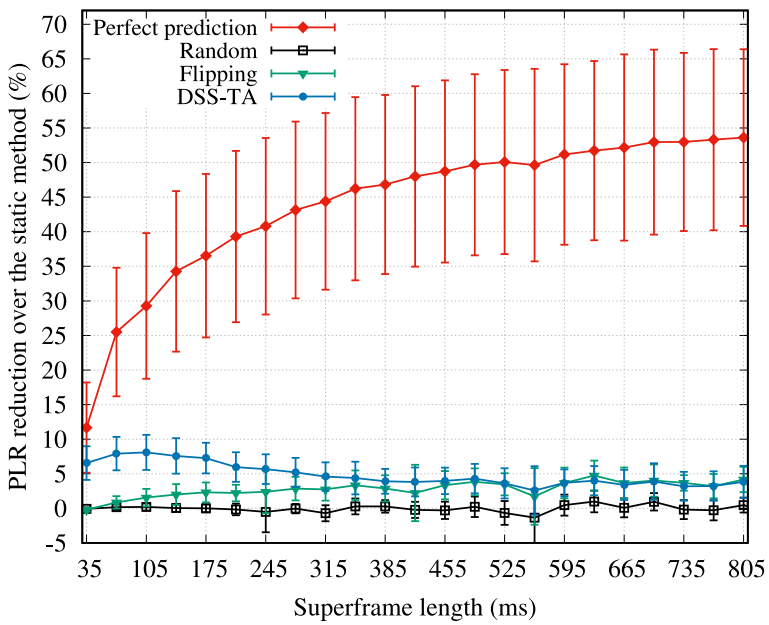

Fig. 15 PLR reduction over the static method vs. superframe length, $P_{Tx} = -15$ dBm

observation indicates that TAM may not provide further accuracy in terms of channel condition prediction when the target future time slot is far away. However, a superframe length longer than 490 ms is normally impractical for most WBAN applications, because even for non-medical applications, the packet latency should be less than 250 ms [43], which limits the superframe to at most 250 ms. Accordingly, except for the applications that are not constrained with respect to packet latency, the DSS-TA provides a more accurate estimation of future channel conditions and hence achieves a better transmission performance in terms of PLR.

6 Conclusions

In this paper, we focus on exploring dynamic slot scheduling (DSS) method in daily activity scenarios for WBAN system. We first collect the realistic on-body channel gain data by using our customized wireless transceivers. Data analyses based on 16 measurements demonstrate that temporal autocorrelation of the on-body channels is significant within a time lag of 500 ms, regardless of the location of transceiver or test subject. Motivated by the significant autocorrelation, we proposed a new slot scheduling method, namely DSS-TA. In DSS-TA, the hub uses a temporal autocorrelation model to predict PLR for future time slots. Then, the slot scheduling problem is transformed into a minimum-cost bipartite matching problem, and the edges in the bipartite are weighted by predicted average PLR. DSS-TA is designed to be compatible with IEEE 802.15.6 standard. We add an extra subslot at the tail of each time slot to keep track the variation of channel gain, and at the beginning of every beacon period, the hub broadcasts the slot scheduling decision to the sensor nodes. To conduct a more real performance evaluation, the real channel realizations are imported into our simulation model to mimic the channel condition variation in the daily life scenarios. Simulation results show that the DSS approach exhibits a great potential in decreasing the PLR for daily scenarios. Moreover, we found superframe length is a key parameter which affects not only the upper bound of DSS method but also the performance of the flipping and DSS-TA methods. There exist a superframe threshold for the flipping and DSS-TA method, when the superframe length is shorter than the threshold, DSS-TA method is more effective than the flipping method; whereas, when the superframe length is longer than the threshold, DSS-TA almost remains the same performance with the flipping method. In the daily activity scenarios, the threshold is around 490 ms. Considering the packet latency requirement for majority WBAN applications is below 250 ms, DSS-TA is a more feasible choice. We also explore the effect of Tx power level on the sensor side. The Tx power level is a key parameter affecting both PLR and energy consumption, DSS method may provide a new insight to balance the trade-off between transmission reliability and energy consumption. In this paper, all sensor nodes are assumed to have the same Tx power level. The combination of adaptive transmission power control and DSS methods remain as our future works. Besides, with the introducing of extra subslot in each time slot, the extra energy consumption and control overhead is inevitably, even though the cost is little. How to reduce the cost in the sensor side while retaining the effectiveness of DSS is another future work.

Abbreviations

The following abbreviations are used throughout this paper. Some special abbreviations will be defined when they are first used.
ADC: Adaptive duty cycle; BAN: Body area network; CSMA/CA: Carrier sense multiple access/collision avoidance; DSS: Dynamic slot scheduling; IEEE: Institute of electrical and electronics engineers; ISM: Industrial, scientific and medical; MAC: Media access control; MAP: Managed access phase; PLR: Packet loss ratio; QoS: Quality of service; RAP: Random access phase; RSSI: Received signal strength indicator; SUI: Scheduled upload interval; TAM: Temporal autocorrelation model; TDMA: Time-division multiple access; TPC: Transmission power control; WBAN: Wireless body area network; WSS: Wide sense stationary

Availability of data and materials

All channel gain datasets are collected from our customized wireless transceivers. For the time being, we do not wish to share our data, as our current project still relies on these datasets.

Authors' contributions

HZ contributed the central idea, collected and analyzed the data, and wrote the initial draft of the paper. All authors contributed to refining the ideas, carrying out additional analyses, and finalizing this paper. All authors read and approved the final manuscript.

Competing interests

The authors declare that they have no competing interests.

Publisher's Note

Received: 17 January 2018 Accepted: 28 September 2018
Published online: 20 October 2018

References

1. IEEE Standards Association, IEEE Standard for Local and Metropolitan Area Networks—part 15.6: Wireless Body Area Networks. IEEE
2. K.Y. Yazdandoost, K. Sayrafian-Pour, Channel model for body area network (BAN). IEEE P802.15.6 (2009)
3. M. Sudjai, T. Le Chung, F. Safaei, in *Proc. IEEE International Symposium on Personal Indoor and Mobile Radio Communications (PIMRC)*. Performance analysis of STFC MB-OFDM UWB in WBAN channels, (2012), pp. 1710–1715
4. L.C. Tran, A. Mertins, X. Huang, F. Safaei, Comprehensive performance analysis of fully cooperative communication in WBANs. IEEE Access. **4**, 8737–8756 (2016)
5. M. Sudjai, L.C. Tran, F. Safaei, On the energy efficiency of adaptive WBAN systems for mhealth services. EAI Endorsed Trans. Pervasive Health Technol. **17**(9), 1–12 (2017)
6. H. Zhang, F. Safaei, L.C. Tran, in *Proc. IEEE Symposium on Computers and Communication (ISCC)*. Joint analog network coding and channel allocation in the walking scenario for WBAN, (2016), pp. 604–609
7. H. Zhang, F. Safaei, L.C. Tran, A novel cooperation-based network coding scheme for walking scenarios in WBANs. Wirel. Commun. Mob. Comput. **2017**, 1–20 (2017)

8. H. Zhang, F. Safaei, L.C. Tran, in *Proc. IEEE Vehicular Technology Conference (VTC Spring)*. Measurement-based characterizations of on-body channel in the human walking scenario, (2017), pp. 1–5
9. A. Boulis, D. Smith, D. Miniutti, L. Libman, Y. Tselishchev, Challenges in body area networks for healthcare: the MAC. IEEE Commun. Mag. **50**(5), 100–106 (2012)
10. L.W. Hanlen, D. Miniutti, D. Rodda, B. Gilbert, in *Proc. IEEE International Symposium on Personal, Indoor and Mobile Radio Communications (PIMRC)*. Interference in body area networks: distance does not dominate, (2009), pp. 281–285
11. J. Zhang, D. B. Smith, L.W. Hanlen, D. Miniutti, D. Rodda, B. Gilbert, Stability of narrowband dynamic body area channel. IEEE Antennas Wirel. Propag. Lett. **8**, 53–56 (2009)
12. A. Farhad, Y. Zia, S. Farid, F.B. Hussain, D-MAC: a dynamic MAC algorithm for the body area sensor networks based on ieee 802.15. 4. Int. J. Comput. Sci. Netw. Secur. **16**(5), 29 (2016)
13. M.M. Alam, E.B. Hamida, O. Berder, D. Menard, O. Sentieys, A heuristic self-adaptive medium access control for resource-constrained wban systems. IEEE Access. **4**, 1287–1300 (2016)
14. M.S. Akbar, H. Yu, S. Cang, TMP: tele-medicine protocol for slotted 802.15.4 with duty-cycle optimization in wireless body area sensor networks. IEEE Sensors J. **17**(6), 1925–1936 (2017)
15. H. Alshaheen, H.T. Rizk, in *Proc. IEEE Wireless Communications and Mobile Computing Conference (IWCMC)*. Improving the energy efficiency for a WBSN based on a coordinate duty cycle and network coding, (2017), pp. 1215–1220
16. S. Xiao, A. Dhamdhere, V. Sivaraman, A. Burdett, Transmission power control in body area sensor networks for healthcare monitoring. IEEE J. Sel. Areas Commun. **27**(1), 37–48 (2009)
17. W. Gao, B. Jiao, G. Yang, W. Hu, J. Liu, Transmission power control for IEEE 802.15.6 body area networks. ETRI J. **36**(2), 313–316 (2014)
18. S. Archasantisuk, T. Aoyagi, M. Kim, J.i. Takada, in *Proc. IEEE Annual International Symposium on Personal, Indoor, and Mobile Radio Communications (PIMRC)*. Transmission power control in WBAN using the context-specific temporal correlation model, (2016), pp. 1–6
19. A. H. Sodhro, Y. Li, M. A. Shah, Energy-efficient adaptive transmission power control for wireless body area networks. IET Commun. **10**(1), 81–90 (2016)
20. H. Moosavi, F.M. Bui, Optimal relay selection and power control with quality-of-service provisioning in wireless body area networks. IEEE Trans. Wireless Commun. **15**(8), 5497–5510 (2016)
21. D.B. Smith, L.W. Hanlen, D. Miniutti, in *Proc. IEEE Wireless Communications and Networking Conference (WCNC)*. Transmit power control for wireless body area networks using novel channel prediction, (2012), pp. 684–688
22. W. Zang, S. Zhang, Y. Li, An accelerometer-assisted transmission power control solution for energy-efficient communications in WBAN. IEEE J. Sel. Areas Commun. **34**(12), 3427–3437 (2016)
23. A. Asadi, V. Mancuso, A survey on opportunistic scheduling in wireless communications. IEEE Commun. Surveys Tuts. **15**(4), 1671–1688 (2013)
24. Y. Tselishchev, L. Libman, A. Boulis, in *Proc. IEEE International Symposium on a World of Wireless, Mobile and Multimedia Networks (WoWMoM)*. Reducing transmission losses in body area networks using variable TDMA scheduling, (2011), pp. 1–10
25. Y. Tselishchev, A. Boulis, L. Libman, Variable scheduling to mitigate channel losses in energy-efficient body area networks. Sensors. **12**(11), 14692–14710 (2012)
26. E.N. Gilbert, Capacity of a burst-noise channel. Bell Labs Tech. J. **39**(5), 1253–1265 (1960)
27. Y. Zhou, Z. Sheng, V.C.M. Leung, P. Servati, in *Proc. IEEE Annual International Conference of the Engineering in Medicine and Biology Society (EMBC)*. Beacon-based opportunistic scheduling in wireless body area network, (2016), pp. 4995–4998
28. R. Pan, D. Chua, J.S. Pathmasuntharam, Y. P. Xu, An opportunistic relay protocol with dynamic scheduling in wireless body area sensor network. IEEE Sensors J. **15**(7), 3743–3750 (2015)
29. Z. Yan, B. Liu, C.W. Chen, in *Proc. IEEE International Conference on e-Health Networking, Applications and Services (Healthcom)*. QoS-driven scheduling approach using optimal slot allocation for wireless body area networks, (2012), pp. 267–272
30. B. Liu, Z. Yan, C.W. Chen, MAC protocol in wireless body area networks for e-health: challenges and a context-aware design. IEEE Wirel. Commun. **20**(4), 64–72 (2013)
31. B. Liu, Z. Yan, C.W. Chen, Medium access control for wireless body area networks with QoS provisioning and energy efficient design. IEEE Trans. Mob. Comput. **16**(2), 422–434 (2017)
32. V. Chaganti, L. Hanlen, D. Smith, Are narrowband wireless on-body networks wide-sense stationary? IEEE Trans. Wireless Commun. **13**(5), 2432–2442 (2014)
33. D.B. Smith, J. Zhang, L.W. Hanlen, D. Miniutti, D. Rodda, B. Gilbert, Temporal correlation of dynamic on-body area radio channel. Electron. Lett. **45**(24), 1212–1213 (2009)
34. L. Hanlen, V. Chaganti, B. Gilbert, D. Rodda, T. Lamahewa, D.B. Smith, in *Proc. IEEE International Symposium on Personal, Indoor and Mobile Radio Communications Workshops (PIMRC)*. Open-source testbed for body area networks: 200 sample/sec, 12 hrs continuous measurement, (2010), pp. 66–71
35. M. Lauzier, P. Ferrand, A. Fraboulet, H. Parvery, J.M. Gorce, in *Proc. European Conference on Antennas and Propagation (EuCAP)*. Full mesh channel measurements on body area networks under walking scenarios, (2013), pp. 3508–3512
36. R. D'Errico, L. Ouvry, in *Proc. IEEE International Symposium on Personal, Indoor and Mobile Radio Communications (PIMRC)*. Time-variant BAN channel characterization, (2009), pp. 3000–3004
37. A. Fort, C. Desset, P. Wambacq, L.V. Biesen, Indoor body-area channel model for narrowband communications. IET Microwaves Antennas Propag. **1**(6), 1197–1203 (2007)
38. V.G. Chaganti, D.B. Smith, L.W. Hanlen, Second-order statistics for many-link body area networks. IEEE Antennas Wirel. Propag. Lett. **9**, 322–325 (2010)
39. H. Feng, B. Liu, Z. Yan, C. Zhang, C.W. Chen, in *Proc. IEEE International Symposium on Personal, Indoor, and Mobile Radio Communications (PIMRC)*. Prediction-based dynamic relay transmission scheme for wireless body area networks, (2013), pp. 2539–2544
40. H.W. Kuhn, The Hungarian method for the assignment problem. Nav. Res. Logist. **2**(1-2), 83–97 (1955)
41. A. Boulis, Castalia: A simulator for wireless sensor networks and body area networks. https://github.com/boulis/Castalia/. Accessed 12 Oct 2018
42. Texas Instuments, 2.4 GHz IEEE 802.15.4/zigbee-ready RF transceiver. http://www.ti.com/lit/ds/symlink/cc2420.pdf. Accessed 12 Oct 2018
43. D.B. Smith, D. Miniutti, T.A. Lamahewa, L.W. Hanlen, Propagation models for body-area networks: a survey and new outlook. IEEE Antennas Propag. Mag. **55**(5), 97–117 (2013)